

# Stability Analysis of Interface Conditions for Ocean-Atmosphere Coupling

Hong Zhang · Zhengyu Liu · Emil Constantinescu · Robert Jacob

Preprint ANL/MCS-P9224-0819

Received: date / Accepted: date

**Abstract** In this paper we analyze the stability of different coupling strategies for multidomain PDEs that arise in general circulation models used in climate simulations. We focus on fully coupled ocean-atmosphere models that are needed to represent and understand the complicated interactions of these two systems, becoming increasingly important in climate change assessment in recent years. Numerical stability issues typically arise because of different time-stepping strategies applied to the coupled PDE system. In particular, the contributing factors include using large time steps, lack of accurate interface flux, and single-iteration coupling. We investigate the stability of the coupled ocean-atmosphere models for various interface conditions such as the Dirichlet-Neumann condition and the bulk interface condition, which is unique to climate modeling. By analyzing a simplified

---

This material is based upon work supported by the U.S. Department of Energy, Office of Science, Office of Advanced Scientific Computing Research and Office of Biological and Environmental Research, Scientific Discovery through Advanced Computing (SciDAC) program under contract DE-AC02-06CH11357 through the Coupling Approaches for Next-Generation Architectures (CANGA) project.

✉H. Zhang  
Mathematics and Computer Science Division  
Argonne National Laboratory, Lemont, IL  
E-mail: hongzhang@anl.gov

Z. Liu  
Department of Geography  
Ohio State University, Columbus, OH  
E-mail: liu.7022@osu.edu

E. Constantinescu  
Mathematics and Computer Science Division  
Argonne National Laboratory, Lemont, IL  
E-mail: emconsta@anl.gov

R. Jacob  
Environmental Science Division  
Argonne National Laboratory, Lemont, IL  
E-mail: jacob@anl.gov

model, we demonstrate how the parameterization of the bulk condition and other numerical and physical parameters affect the coupling stability.

**Keywords** stability analysis, coupled system, partitioned algorithm, ocean-atmosphere

**Mathematics Subject Classification (2010)** 65M12, 34D20, 76R50

## 1 Introduction

We analyze the stability of different coupling strategies for multidomain partial differential equations (PDEs) motivated by general circulation models used in climate simulations. Solving these problems with large time steps on each of the domains is known to cause numerical stability issues of the coupled PDE system. Without loss of generality we consider two coupled PDEs that correspond to coupled ocean-atmosphere:

$$\frac{\partial u_1(t, x)}{\partial t} = F_1(t, u_1(t, x), u_2(t, x)) \quad [\text{domain 1}] \quad (1a)$$

$$\frac{\partial u_2(t, x)}{\partial t} = F_2(t, u_1(t, x), u_2(t, x)) \quad [\text{domain 2}] \quad (1b)$$

$$0 = G_{12}(u_1(t, x), u_2(t, x)), \quad [\text{interface 1-2}] \quad (1c)$$

$$t \geq t_0, u_k \in \mathbb{R} \times \mathcal{D}_k, F_k : \mathbb{R} \times \mathcal{D} \rightarrow \mathcal{D}_k, k = 1, 2$$

$$G_{12} : \mathcal{D} \rightarrow \mathcal{D}, \mathcal{D} = \bigcup_{k=1,2} \mathcal{D}_k$$

where, for instance, (1a) represents the atmosphere, (1b) the ocean, and (1c) the interaction between the two problems. Stability is defined as  $\|u^n(x)\| \leq C\|u(t_0, x)\|$ ,  $\forall n > 0$ , where  $C$  is a finite constant independent of  $t$  and  $u = [u_1, u_2]^T$ .

This problem has been analyzed by normal mode analysis and matrix stability. The normal mode method was originally developed by Godunov and Ryabenkij [17], Kriess [22] and Osher [29], and later led to the theory of Gustafsson, Kriess, and Sundstrom (GKS) [19], which establishes necessary and sufficient conditions that the discretization schemes must satisfy in order to ensure stability. We are interested in utilizing this tool to analyze stability of various interface conditions for coupled climate models.

### 1.1 Scientific application

Coupling methods have been a limiting factor in researchers' ability to address science questions where the relevant processes are strongly coupled. Each model inside the coupled system is often associated with different time scales, posing a great challenge on time integration. The integration is becoming more challenging as the coupled simulation codes are evolving to support high resolution in time and space and concurrent execution of components. While the time integration for each model is often well founded in theory, little work has been done on characterizing the influence of different coupling strategies on the stability of the fully coupled system.

In the U.S. climate community models, including CESM [21] and DOE E3SM [18] (previously known as ACME), the Earth system components (global atmosphere, global ocean, sea ice and land surface) are numerically treated independently. The interaction among these components is done through a component called a “coupler” which accommodates the information exchange. In the E3SM coupler, the components of the Earth system model are marched forward in time nearly independently from each other, with appropriate field information exchanged using the lagged states at the previous time interval, also known as “explicit flux coupling.” While this popular coupling method, really more of a decoupled method, enables concurrent execution of multiple components for computational efficiency, in certain parameter regimes it has been shown to induce numerical instability at the air-sea interface [25], air-land interface [5], and sea-ice interface [20,32]. In the tropics where the atmosphere is very sensitive to the sea surface forcing, the standard coupling strategy that propagates the atmospheric model with multiple small explicit time steps followed by a large ocean time step is physically reasonable [7,30,3]. In other regions such as the extratropics [24], however, the atmospheric forcing is dominated by its own internal variability, providing rapid feedback to the ocean via the turbulent heat flux. Thus, using large time steps for the ocean can be problematic. On long timescales (e.g., more than one year), the standard coupling method fails to produce the correct ocean-atmosphere heat flux both in magnitude and in sign, contributing to poor understanding of climate variability in these regions [24,6,26,28]. In [24], Kushnir et al. concluded that the thermal coupling coefficient should be a function of latitude and season in order to enhance the predictability of extratropical systems.

The occasional failure of decoupled methods can be attributed to the fact that these methods perform a single step of an iterative process [25], which is insufficient to secure stable and accurate solutions. A theoretically ideal solution for stability is to build a monolithic fully coupled system and solve it implicitly. Doing so is difficult, however, because it is intrusive in nature, requiring significant development effort to refactor existing codes; and solving the full implicit system efficiently is also a computational challenge. A more practical approach is for each component to compute interface fluxes using lagged information from the other components and implicitly the states owned by itself. In this way, partial implicitness has been added, thus improving stability without the need for many iterations when compared with explicit flux coupling; but the resulting system is not as stable as the one using full implicitness [25]. Rigorous analysis of decoupled methods remains limited and does not provide sufficient understanding of optimal choices for stability.

To improve the stability of surface models (e.g., snow, ice, or soil) that are coupled to atmospheric models, Beljaars et al. [5] proposed a fully implicit formulation that uses an estimate of the surface temperature at the new time level instead of solving for it. The estimate is obtained with an empirical relation between surface heat flux and surface temperature that is derived from idealized simulations of a fully coupled implicit system. A matrix stability analysis was performed on the forced surface models; however, only an empirical stability condition was given.

The stability limits in fluid-solid interaction (FSI) coupled models have been widely studied, but little is known for climate models that are intrinsically large scale and involve complex dynamics. Recently Connors and his colleagues conducted a series of studies [9,10,11,1] that provide rigorous analysis of various

partitioned algorithms for fluid-fluid interaction with a focus on convergence and accuracy aspects. Peterson [31] et. al. proposed a new synchronous partitioned method that eliminates the need to solve a coupled implicit system, while not subject to additional stability constraints as in traditional partitioned schemes. Although the approach is developed for general transmission problem, it can be potentially extended to coupled climate models.

This work studies the stability of different partitioned coupling methods for ocean-atmosphere coupling, which involves the most computationally expensive components in climate models. We examine the stability behaviors of common interface conditions with a focus on the bulk interface condition that is pervasive in coupled climate models. We show by analysis that partially implicit and fully implicit flux coupling can lead to an unconditionally stable coupling algorithm, whereas explicit flux coupling requires certain Courant-Friedrichs-Lewy (CFL)-like conditions to be satisfied for stability. We also derive the closed-form necessary and sufficient stability condition for a one-way coupled system, and connect one-way and two-way coupled models in terms of stability regions. The theoretical analyses are accompanied by numerical experiments. The new results lead to better understanding of the stability properties of the existing algorithms as well as provide guidance for developing new stable coupling algorithms.

## 1.2 Model problem

Since the vertical diffusion provides the strongest coupling between the atmospheric boundary layer and the ocean, we consider a 1D diffusion equation for temperature defined on two neighboring domains

$$\frac{\partial}{\partial t} T_+ = \frac{\partial}{\partial z} \left( K_+ \frac{\partial}{\partial z} T_+ \right), \quad z > 0 \quad (2a)$$

$$\frac{\partial}{\partial t} T_- = \frac{\partial}{\partial z} \left( K_- \frac{\partial}{\partial z} T_- \right), \quad z < 0 \quad (2b)$$

with the eddy diffusivity coefficient determined by

$$K_{\pm} = \frac{\nu_{\pm}}{\rho_{\pm} c_{\pm}}, \quad (3)$$

where  $\nu$  and  $\rho$  and  $c$  are the heat diffusion coefficient, the density, and the heat capacity, respectively. The subscripts  $+$  and  $-$  correspond to atmosphere and ocean, respectively. In this case  $u_1 = T_+$ ,  $u_2 = T_-$ ,  $\mathcal{D}_1$  is the positive domain, and  $\mathcal{D}_2$  is the negative domain in the (1).

In addition to the governing equations for each subsystem, the continuity of fluxes at the interface is typically used as the coupling condition

$$\rho_+ c_+ K_+ \frac{\partial}{\partial z} T_+ = \rho_- c_- K_- \frac{\partial}{\partial z} T_-, \quad (4)$$

which corresponds to (1c).

Note that the diffusion problem can also be represented in an equivalent form

$$\begin{aligned} \rho_+ c_+ \frac{\partial}{\partial t} T_+ &= \frac{\partial}{\partial z} \left( \nu_+ \frac{\partial}{\partial z} T_+ \right), \quad z > 0 \\ \rho_- c_- \frac{\partial}{\partial t} T_- &= \frac{\partial}{\partial z} \left( \nu_- \frac{\partial}{\partial z} T_- \right), \quad z < 0 \end{aligned}$$

and the flux continuity becomes

$$\nu_+ \frac{\partial}{\partial z} T_+ = \nu_- \frac{\partial}{\partial z} T_-.$$

This alternative form makes the coupling condition simpler, but involves more parameters in the implementation of the subsystems.

### 1.3 Interface conditions

The physical processes in the interior of each domain are independent of the others; each domain-specific process interacts with processes in other domains only at their common interface. Therefore, conditions need to be imposed at the interface in order to guarantee that the numerical solution exists for the coupled system.

In classical domain decomposition methods, both the state and the normal-direction flux often are required to be continuous across the interface. When a partitioned approach is used, each domain is solved independently by using boundary information coming from the other domains. The information is often lagged in time if the domains are solved concurrently. A natural choice for implementing the interface conditions is to treat them as boundary conditions and apply Dirichlet or Neumann conditions to each subproblem.

In a climate model, the surface fluxes of momentum, sensible heat, and latent heat are calculated by using bulk formulas, following the Monin-Obukhov similarity theory [35]. The physical processes near the surface are parameterized as bulk transfer coefficients as studied in classical works [27, 34, 14]. Through bulk transfer coefficients, a bulk formula relates the flux to easily measured surface quantities such as averaged wind speed, temperature, and humidity. The most popular bulk flux algorithm, the Coupled Ocean-Atmosphere Response Experiment (COARE) algorithm [14], has been used in coupled air-sea [3] and sea-ice [2] simulations and has been continuously improved over wider wind-speed range and more complicated physics such as wave feedback [13, 23].

From a mathematical point of view, the bulk flux algorithm can be abstracted as a special type of interface condition: the flux is continuous in the normal direction at the interface, but the state can jump across the interface. Without loss of generality, the bulk interface condition can be described as

$$\nu_+ \frac{\partial}{\partial z} T_+ = \nu_- \frac{\partial}{\partial z} T_- = b(T_+ - T_-) \quad (6)$$

with the bulk coefficient defined as

$$b = \rho_+ c_+ C_H \|U\|, \quad (7)$$

where  $C_H$  is the exchange coefficient at reference height  $r$  (e.g., a typical value is 10 meters) that depends on surface roughness and local stability and  $\|U\|$  is the absolute (wind) velocity. This parameter is defined in a bulk way in the region between the lowest vertical level in the atmospheric model and the shallowest vertical level in the oceanic model. Some authors in literature have described the same interface condition based on a variable  $\alpha$ , which can be related to  $b$  by

$$\alpha = b/(\rho_+ c_+). \quad (8)$$

For the convenience of denoting flux, we prefer the notation  $b$ . But using the other notation should not affect the conclusions reached in this paper.

Consequently, the heat flow at the the interface can be computed as

$$K_+ \frac{\partial}{\partial z} T_+ = \rho_+ c_+ \alpha (T_+ - T_-), \quad K_- \frac{\partial}{\partial z} T_- = \frac{\rho_- c_-}{\rho_+ c_+} \alpha (T_+ - T_-). \quad (9)$$

#### 1.4 Partitioned coupling algorithms

The classical partitioned approach is the convectional serial staggered (CSS) algorithm that solves the two subsystems alternatively. We assume at time  $t_n$  that the temperature fields  $T_j^n$  are given and are consistent at the interface. With a grid setup shown in Figure 1, the algorithm can be described compactly as

$$T_{0+}^n = T_{0-}^n \quad (10a)$$

$$\rho_+ c_+ \frac{\partial}{\partial t} T_j = \frac{\nu_+}{(\Delta z_+)^2} (T_{j+1} - 2T_j + T_{j-1}), \quad j > 0 \quad (10b)$$

$$q_{\frac{1}{2}} = \nu_+ \frac{T_1 - T_{0+}}{\Delta z_+}, \quad q_{-\frac{1}{2}} = \nu_- \frac{T_{0-} - T_{-1}}{\Delta z_-} \quad (10c)$$

$$\frac{1}{2} (\rho_- c_- \Delta z_- + \rho_+ c_+ \Delta z_+) \frac{\partial}{\partial t} T_{0-} = q_{\frac{1}{2}} - q_{-\frac{1}{2}}, \quad j = 0 \quad (10d)$$

$$\rho_- c_- \frac{\partial}{\partial t} T_j = \frac{\nu_-}{(\Delta z_-)^2} (T_{j+1} - 2T_j + T_{j-1}) \quad j < 0. \quad (10e)$$

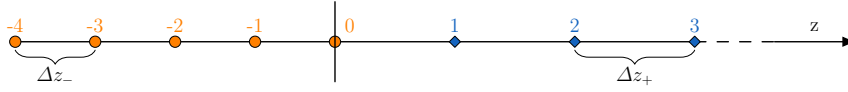


**Fig. 1** Grid setting for Dirichlet-Neumann condition. Space is discretized on uniform grids with each node denoted by  $z_j = j\Delta z_+$   $j = 0, 1, 2, \dots$  and  $z_j = j\Delta z_-$   $j = 0, -1, -2, \dots$  where  $\Delta z_+$  and  $\Delta z_-$  are the grid spacing on the left and right sides of the interface respectively. They may differ significantly.

The procedure to advance the solution from  $t_n$  to  $t_{n+1}$  is as follows:

1. At time  $t_n$ , transfer the temperature  $T_{0-}^n$  to the positive domain, and update its interface boundary with a Dirichlet condition (10a).
2. Advance the solution on the right domain from  $t_n$  to  $t_{n+1}$  (10b), and compute the flux at the interface (10c).
3. Transfer the flux quantifies to the left domain, and update its interface boundary with a Neumann condition (10d).
4. Advance the solution on the left domain (10e)

This algorithm can also be applied to Neumann-Neumann or bulk interface conditions with a slightly different grid setting, as shown in Figure 2. For the convenience of flux calculation, the interface is positioned at the cell edge for both domains; in this way, each subdomain can have uniform cells, but ghost cells need

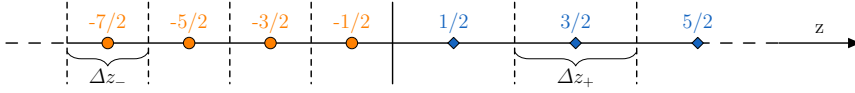


**Fig. 2** Grid setting for bulk and Neumann-Neumann interface conditions. Space is discretized on uniform grids with each node denoted by  $z_{j+1/2} = (j + 1/2)\Delta z_+$   $j = 0, 1, 2, \dots$  and  $z_{j+1/2} = (j + 1/2)\Delta z_-$   $j = -1, -2, \dots$  where  $\Delta z_+$  and  $\Delta z_-$  are the grid spacing on the left and right sides of the interface respectively. They may differ significantly.

to be used to apply the boundary conditions at the interface. We denote the ghost cell values for the left and the right domains by  $T_{0+}$  and  $T_{0-}$ , respectively.

After spatial discretization, the following system of ordinary differential equations is obtained:

$$q_{0+} = b(T_{\frac{1}{2}} - T_{-\frac{1}{2}}) \quad (11a)$$

$$\frac{\partial}{\partial t} T_{j+\frac{1}{2}} = \frac{1}{\rho_+ c_+ \Delta z_+} (q_{j+1} - q_j), \quad j \geq 0 \quad (11b)$$

$$q_{0-} = q_{0+} \quad (11c)$$

$$\frac{\partial}{\partial t} T_{j+\frac{1}{2}} = \frac{1}{\rho_- c_- \Delta z_-} (q_{j+1} - q_j), \quad j < 0. \quad (11d)$$

For simplicity, we will focus on backward Euler when referring to the implicit time stepping method, unless otherwise noted. Extending to high-order time integration schemes is possible but complicates the algebraic analysis considerably.

## 1.5 Manuscript organization

The rest of this paper is organized as follows. Normal mode stability analysis for two-way coupled models using Dirichlet-Neumann and bulk interface conditions is given in Sections 2 and 3. Section 4 applies the analysis to a one-way coupled model that can be considered as a limiting case for two-way coupled models. Section 5 describes how to validate the analysis using matrix stability and provides the numerical results. In Section 6, we summarize the results and their implications to practical applications.

## 2 Normal mode stability analysis for Dirichlet-Neumann condition

In the normal mode method, the PDE solution is represented as a certain mode, which is typically exponential in time and space. For example, the numerical solution of one-dimensional PDE can be assumed in the form

$$T_j^b = \mathcal{A}^n \phi_j, \quad (12)$$

where  $\mathcal{A}$  is an eigenvalue with eigenfunction  $\phi_j$  (bounded as  $j$  goes to infinity). Then one needs to solve a system of algebraic equations, resulting directly from numerical discretization and boundary (or interface) conditions, for the amplitude of the mode.

Based on this technique, the GKS theory [19] establishes a necessary and sufficient condition for stability, as summarized below.

**Proposition 1** *The approximation scheme is stable in the GKS sense if and only if no nontrivial eigensolution exists for  $|\mathcal{A}| \geq 1$ .*

The stability definition is given in Definition 3.3 in [19], and Proposition 1 refers to Theorem 5.1 in Section 5 in [19]. Although the original theory was described for quarter-plane problems, it can be naturally applied to problems with multiple boundaries and interface problems such as FSI.

Giles has shown in [16] that for FSI problems that the key point to achieving numerical stability is to transfer the interface temperature from the solid to the fluid (Dirichlet condition) and to pass the heat flux (Neumann condition) from the fluid to the solid. Roux and Garaud confirmed in [33] that Dirichlet conditions must be imposed in the domain with lower conductivity.

Lemarie et al. also followed Giles' partitioned approach in [25]. The main difference between Giles' approach and the one considered in this paper is the former is derived based on an engineering consideration—a half-sized cell is used at the interface so that each domain can be treated independently. Consequently, the partitioned approach solves a slightly different model from the one targeted by a monolithic approach. In this section, we present a normal mode analysis for a partitioned approach without using half-sized cell. Both explicit and implicit time-stepping schemes will be considered in order to provide a direct comparison with results in [16].

## 2.1 Explicit flux coupling with explicit time stepping

Following the explicit methods (as opposed to implicit) of Giles [16], we calculate the interfacial flux (10c) for the time step from  $t_n$  with

$$q_{\frac{1}{2}}^n = \nu_+ \frac{T_1^n - T_{0+}^n}{\Delta z_+}, \quad q_{-\frac{1}{2}}^n = \nu_- \frac{T_{0-}^n - T_{-1}^n}{\Delta z_-} \quad (13)$$

and assume a solution of the form

$$T_j^n = \begin{cases} \mathcal{A}^n \kappa_-^j, & j = 0, -1, -2, \dots \\ \mathcal{A}^n \kappa_+^j, & j = 1, 2, \dots, \end{cases} \quad (14)$$

where  $j$  denotes exponent,  $\kappa^j$  are bounded functions of space, and  $\mathcal{A}$  is a complex scalar. We define the following constants:

$$r = \frac{\rho_+ c_+ \Delta z_+}{\rho_- c_- \Delta z_-}, \quad d_{\pm} = \frac{\nu_{\pm} \Delta t}{\rho_{\pm} c_{\pm} (\Delta z_{\pm})^2}. \quad (15)$$

Discretizing (10) explicitly with the coupling flux being computed according to the formula (13), substituting the solution (14) into the discretized equations, and using (15) to simplify expression, we have

$$\mathcal{A} = 1 + d_+ (\kappa_+ - 2 + \kappa_+^{-1}) \quad (16a)$$

$$(\mathcal{A} - 1)(1 + r) = 2d_+ r (\kappa_+ - 1) - 2d_- (1 - \kappa_-^{-1}) \quad (16b)$$

$$\mathcal{A} = 1 + d_- (\kappa_- - 2 + \kappa_-^{-1}). \quad (16c)$$

Then (16a) leads to

$$\kappa_+^2 - \left(2 + \frac{\mathcal{A} - 1}{d_+}\right) \kappa_+ + 1 = 0. \quad (17)$$

In the region  $|\mathcal{A}| > 1$ , there are two roots, and their product is 1; thus, one of the two roots must meet  $|\kappa_+| > 1$  and the other must meet  $|\kappa_+| < 1$ . We are interested only in the latter, so that the far-field boundary condition is satisfied. Thus, we pick the solution

$$\kappa_+ = 1 + \frac{\mathcal{A} - 1}{2d_+} \left(1 - \sqrt{1 + \frac{4d_+}{\mathcal{A} - 1}}\right). \quad (18)$$

Similarly for (16c) we choose the solution

$$\kappa_-^{-1} = 1 + \frac{\mathcal{A} - 1}{2d_-} \left(1 - \sqrt{1 + \frac{4d_-}{\mathcal{A} - 1}}\right). \quad (19)$$

Plugging these into (16b) and simplifying the expression, we obtain

$$1 + r = \left(1 - \sqrt{1 + \frac{4d_-}{\mathcal{A} - 1}}\right) + r \left(1 - \sqrt{1 + \frac{4d_+}{\mathcal{A} - 1}}\right). \quad (20)$$

When  $\mathcal{A}$  is real, the radicals must be zero. And the requirement that  $\mathcal{A} \leq 1$  leads to  $0 < d_+, d_- \leq \frac{1}{2}$ , which agrees with the classical CFL condition that can be obtained by applying von Neumann stability analysis to an uncoupled system. If  $\mathcal{A}$  is complex, the imaginary parts of the two terms on the right-hand side must cancel out, and their real parts must be zero. Thus the radicals must be real, which contradicts with the assumption. Hence, there is no stability loss in the coupling, and stability is guaranteed when classical CFL conditions are satisfied on each domain regardless of the value of  $r$ .

## 2.2 Explicit flux coupling with implicit time stepping

Solving the interior equations implicitly and updating the interface data explicitly, we have the following algorithm:

$$T_{0_+}^{n+1} = T_{0_-}^n \quad (21a)$$

$$T_j^{n+1} - T_j^n = \frac{\Delta t \nu_+}{\rho_+ c_+ (\Delta z_+)^2} \left(T_{j+1}^{n+1} - 2T_j^{n+1} + T_{j-1}^{n+1}\right), \quad j > 0 \quad (21b)$$

$$T_{0_-}^{n+1} - T_{0_-}^n = \frac{2\Delta t}{\rho_- c_- \Delta z_- + \rho_+ c_+ \Delta z_+} \left(\nu_+ \frac{T_1^n - T_{0_+}^n}{\Delta z_+} - \nu_- \frac{T_{0_-}^{n+1} - T_{-1}^{n+1}}{\Delta z_-}\right) \quad (21c)$$

$$T_j^{n+1} - T_j^n = \frac{\Delta t \nu_-}{\rho_- c_- (\Delta z_-)^2} \left(T_{j+1}^{n+1} - 2T_j^{n+1} + T_{j-1}^{n+1}\right), \quad j < 0. \quad (21d)$$

Assume a solution is of the form

$$T_j^n = \begin{cases} \mathcal{A}^n \kappa_-^j, & j = 0_-, -1, -2, \dots \\ \mathcal{A}^{n-1} \kappa_+^j, & j = 0_+, 1, 2, \dots \end{cases}$$

so that (21a) is automatically satisfied by this choice of normal mode. The other three equations require that  $\mathcal{A}$ ,  $\kappa_-$ , and  $\kappa_+$  satisfy

$$\begin{aligned} 1 &= \mathcal{A}^{-1} + d_+(\kappa_+ - 2 + \kappa_+^{-1}) \\ (1 - \mathcal{A}^{-1})(1 + r) &= 2d_+r\mathcal{A}^{-2}(\kappa_+ - 1) - 2d_-(1 - \kappa_-^{-1}) \\ 1 &= \mathcal{A}^{-1} + d_-(\kappa_- - 2 + \kappa_-^{-1}). \end{aligned} \quad (22)$$

The first equation leads to

$$\kappa_+^2 - \left(2 + \frac{1 - \mathcal{A}^{-1}}{d_+}\right) \kappa_+ + 1 = 0. \quad (23)$$

In the region  $|\mathcal{A}| > 1$ , there are two real roots with one of them being  $|\kappa_+| > 1$  and the other being  $|\kappa_+| < 1$ . Again we choose the latter, which can be written as

$$\kappa_+ = 1 + \frac{1 - \mathcal{A}^{-1}}{2d_+} \left(1 - \sqrt{1 + \frac{4d_+}{1 - \mathcal{A}^{-1}}}\right). \quad (24)$$

The third equation gives

$$\kappa_-^{-1} = 1 + \frac{1 - \mathcal{A}^{-1}}{2d_-} \left(1 - \sqrt{1 + \frac{4d_-}{1 - \mathcal{A}^{-1}}}\right). \quad (25)$$

Plugging these expressions into the second equation in (22) gives

$$(1 - \mathcal{A}^{-1})(1 + r) = 2d_+r\mathcal{A}^{-2} \left( \frac{1 - \mathcal{A}^{-1}}{2d_+} \left(1 - \sqrt{1 + \frac{4d_+}{1 - \mathcal{A}^{-1}}}\right) \right) - 2d_- \left( -\frac{1 - \mathcal{A}^{-1}}{2d_-} \left(1 - \sqrt{1 + \frac{4d_-}{1 - \mathcal{A}^{-1}}}\right) \right), \quad (26)$$

which simplifies to

$$1 + r = r\mathcal{A}^{-2} \left(1 - \sqrt{1 + \frac{4d_+}{1 - \mathcal{A}^{-1}}}\right) + \left(1 - \sqrt{1 + \frac{4d_-}{1 - \mathcal{A}^{-1}}}\right). \quad (27)$$

Again, we consider asymptotic solutions.

- If  $\Delta z_+ \ll \Delta z_-$ , then  $r \rightarrow 0$ . In this case, we are left with  $\sqrt{1 + \frac{4d_-}{1 - \mathcal{A}^{-1}}} \approx 0$ . Solving for  $\mathcal{A}$  yields  $|\mathcal{A}| \approx \frac{1}{4d_- + 1} < 1$ . It follows that the scheme is unconditionally stable.
- If  $\Delta z_- \ll \Delta z_+$ , then  $r \rightarrow \infty$ . In this case, we have

$$1 \approx \mathcal{A}^{-2} - \mathcal{A}^{-2} \sqrt{1 + \frac{4d_+}{1 - \mathcal{A}^{-1}}}.$$

After some algebra, it follows that  $\mathcal{A}(-\mathcal{A}^4 + \mathcal{A}^3 + 2\mathcal{A}^2 - 2\mathcal{A} + 4d_+) \approx 0$ . Consider a special case  $d_+ = 1$ . We can easily find that all four nonzero roots have a magnitude larger than one. Thus, the scheme is not unconditionally stable. This is an interesting conclusion in an extreme scenario and will be further examined in the next section.

### 2.3 Discussion and comparison with Giles' results

Giles considered a slightly different partitioned approach in [16]. In his approach, (10d) is replaced with

$$\frac{1}{2}\rho_-c_- \Delta z_- \frac{\partial}{\partial t} T_{0_-} = q_0 - q_{-\frac{1}{2}}, \quad j = 0, \quad (28)$$

where  $q_0$  is computed in the same way as  $q_{\frac{1}{2}}$  in (10c) but deemed a one-sided approximation of the flux at the interface. The formula is derived by using finite volume scheme over the half-sized cell  $[z_{-\frac{1}{2}}, 0]$ . By comparing (28) with (10d), we can see that the only difference is the omission of  $\rho_+c_+\Delta z_+$ . The impact on stability seems to depend on how  $\Delta z_+$  compares with  $\Delta z_-$ . Thus, Giles related the coupling stability to the parameter  $r$  in (15) and investigated three algorithms: an explicit algorithm, an implicit algorithm, and a hybrid algorithm (treating one domain explicitly and the other domain implicitly). For all the algorithms, the following conclusions were drawn:

- When  $r \ll 1$ , the coupling is stable.
- When  $r \gg 1$ , the coupling is unstable.
- The stability condition is

$$r < \frac{1 - 2d_-}{1 - \sqrt{1 - 2}}, \quad (29)$$

where  $d$  is the Courant number  $v\Delta t/\Delta z^2$ . Note that this is established under the assumption that Dirichlet boundary condition is used on the positive domain (usually represents fluid) and the Neumann boundary condition is used on the other (usually representing a solid). In practice, the fluid computation has higher resolution than the solid computation has, leading to a stable coupling. But if one uses the Dirichlet boundary condition for the solid and the Neumann boundary condition for the fluid,  $r$  is the inverse of the original quantity and have a very large value. Then the coupling is not stable unless extremely small stepsize is used.

- The stability can be improved by using backward Euler for  $j \leq 0$ . The stability condition would be

$$r < \frac{1 + 2d_-}{1 - \sqrt{1 - 2d_+}}. \quad (30)$$

- If both domains are treated implicitly but the interface data is explicitly updated (e.g., using time lagged information to promote parallelism), the asymptotic stability condition for  $d_-, d_+ \gg 1$  becomes

$$r < \sqrt{\frac{d_-}{d_+}}. \quad (31)$$

In contrast, we consider contributions from both domains for the interface node. The analysis of the explicit algorithm with explicit flux coupling shows that the coupling stability is not affected by  $r$  in our setup for the interface node. For the implicit algorithm (10), our analysis leads to the same conclusions as Giles predicted; however, the causes of instability in the two algorithms are different. In Giles' algorithm, the contribution from the dominant domain (positive domain if  $r \gg 1$ ) is not fully accounted for at the interface since the term  $\rho_+c_+\Delta z_+$  is

missing. With the influence of this missing term excluded, it is easier to see in our framework that the explicit coupling flux passed to the negative domain as Neumann boundary condition dominates the right-hand side of (21c), changing the discretization of this equation from a hybrid scheme to an explicit scheme. To summarize the new findings, the choice of Dirichlet condition or Neumann condition on each domain is important in order to determine the coupling stability when explicit updating of the interfacial flux is used in implicit methods, but it plays no role for purely explicit algorithms.

### 3 Normal mode stability analysis for bulk interface condition

We have shown that even using an implicit time-stepping Dirichlet-Neumann condition and explicit flux coupling can lead to instability, regardless of how the interface condition is imposed at the interface. In this section, we show how the stability properties of the coupling methods are affected in several ways where the interfacial flux (11a) is computed when the bulk interface condition is imposed. In order to relax the stability constraint due to explicit flux coupling, a natural choice is to add implicitness. Thus, we consider the following algorithms based on the degree of implicitness used in the flux computation:

1. Explicit flux coupling

$$q_{0+}^{n+1} = b(T_{\frac{1}{2}}^n - T_{-\frac{1}{2}}^n). \quad (32)$$

2. Partially implicit flux coupling

$$q_{0+}^{n+1} = b(T_{\frac{1}{2}}^{n+1} - T_{-\frac{1}{2}}^n). \quad (33)$$

3. Implicit flux coupling

$$q_{0+}^{n+1} = b(T_{\frac{1}{2}}^{n+1} - T_{-\frac{1}{2}}^{n+1}). \quad (34)$$

Explicit flux coupling and partial flux coupling are convenient for parallel computing and easy to implement, requiring minimal modifications to existing codes that support the Neumann boundary condition. Data transfer between the coupling components is needed only at the beginning of a time step; the frequency is determined by the larger of the stepsizes for each model. The fully implicit treatment of the interfacial flux requires the solution of a monolithic system, which normally indicates more data exchange and synchronization and, more important, tremendous difficulties in developing partitioned algorithms that can solve the equations in both domains simultaneously. However, a sequentially implicit formulation (e.g., [15]) allows the monolithic system to be solved in a partitioned manner (as described by the CSS algorithm (10)), while maintaining the same stability as a fully implicit method [15]. This strategy has been widely used for loosely coupled problems and has a rich literature (e.g., [8, 4, 12]). Since the stability for the fully implicit case is obvious, the analysis will not be repeated in this paper.

### 3.1 Explicit flux coupling with implicit time stepping

Applying backward Euler to the equation (11) gives

$$q_{0+}^{n+1} = b(T_{\frac{1}{2}}^n - T_{-\frac{1}{2}}^n) \quad (35a)$$

$$T_{j+\frac{1}{2}}^{n+1} - T_{j+\frac{1}{2}}^n = \frac{\Delta t}{\rho_+ c_+ \Delta z_+} (q_{j+1}^{n+1} - q_j^{n+1}), \quad j \geq 0 \quad (35b)$$

$$q_{0-}^{n+1} = q_{0+}^n \quad (35c)$$

$$T_{j+\frac{1}{2}}^{n+1} - T_{j+\frac{1}{2}}^n = \frac{\Delta t}{\rho_- c_- \Delta z_-} (q_{j+1}^{n+1} - q_j^{n+1}), \quad j < 0. \quad (35d)$$

The two equations at the interface are

$$T_{\frac{1}{2}}^{n+1} - T_{\frac{1}{2}}^n = \frac{\Delta t}{\rho_+ c_+ \Delta z_+} \left( \nu_+ \frac{T_{\frac{3}{2}}^{n+1} - T_{\frac{1}{2}}^{n+1}}{\Delta z_+} - b(T_{\frac{1}{2}}^n - T_{-\frac{1}{2}}^n) \right) \quad (36a)$$

$$T_{-\frac{1}{2}}^{n+1} - T_{-\frac{1}{2}}^n = \frac{\Delta t}{\rho_- c_- \Delta z_-} \left( b(T_{\frac{1}{2}}^n - T_{-\frac{1}{2}}^n) - \nu_- \frac{T_{-\frac{1}{2}}^{n+1} - T_{-\frac{3}{2}}^{n+1}}{\Delta z_-} \right) \quad (36b)$$

We consider the normal mode solution

$$T_{j+\frac{1}{2}}^n = \begin{cases} \mathcal{A}^n \kappa_-^j, & j = -1, -2, \dots \\ \mathcal{A}^n \kappa_+^{j+1}, & j = 0, 1, 2, \dots \end{cases} \quad (37)$$

Substituting it into Equation (35), we have

$$\begin{aligned} 1 - \mathcal{A}^{-1} &= d_+(\kappa_+ - 2 + \kappa_+^{-1}) \\ 1 - \mathcal{A}^{-1} &= d_+(\kappa_+ - 1) - d_+ \Delta z_+ b / \nu_+ \mathcal{A}^{-1} (1 - \kappa_-^{-1} \kappa_+^{-1}) \\ 1 - \mathcal{A}^{-1} &= d_- \Delta z_- b / \nu_- \mathcal{A}^{-1} (\kappa_+ \kappa_- - 1) - d_- (1 - \kappa_-^{-1}) \\ 1 - \mathcal{A}^{-1} &= d_-(\kappa_- - 2 + \kappa_-^{-1}), \end{aligned} \quad (38)$$

where the second and the fourth equations correspond to the cases  $j = 0$  and  $j = -1$  in (35), respectively. Solving the first and the last equations for  $\kappa_+$  and  $\kappa_-$ , respectively, and choosing the proper roots as before, we get

$$\begin{aligned} \kappa_+ &= 1 + s_+ - \sqrt{s_+^2 + 2s_+} \\ \kappa_-^{-1} &= 1 + s_- - \sqrt{s_-^2 + 2s_-}, \end{aligned} \quad (39)$$

where

$$s_{\pm} = \frac{1 - \mathcal{A}^{-1}}{2d_{\pm}}. \quad (40)$$

The second and third equations of (38) lead to

$$\mathcal{A} = \frac{1 + \beta_+ (1 - \kappa_-^{-1} \kappa_+^{-1})}{1 - d_+ (\kappa_+ - 1)} \quad (41)$$

and

$$\mathcal{A} = \frac{1 + \beta_- (1 - \kappa_- \kappa_+)}{1 - d_- (\kappa_-^{-1} - 1)}, \quad (42)$$

respectively, where for notational convenience we define

$$\beta_{\pm} = \frac{b\Delta t}{\rho_{\pm} c_{\pm} \Delta z_{\pm}} \quad (43)$$

and refer to it as *bulk Courant number*, considering its similarity to classical Courant numbers.

Plugging (39) into (41) and (42) would result in equations that take  $\mathcal{A}$  as functions of  $\beta_{\pm}$  and  $d_{\pm}$ , but there are no closed-form solutions. Thus we consider the asymptotic behavior when  $\beta_+$  approaches zero. Equation (41) becomes

$$\mathcal{A} = \frac{1}{1 - d_+ (\kappa_+ - 1)}. \quad (44)$$

Plugging (39) into it and simplifying lead to

$$\mathcal{A} d_+ (\mathcal{A} - 1) = 0. \quad (45)$$

Therefore  $\mathcal{A} = 1$ , which implies that the system is stable. Similarly with (42), we can see the system is stable when  $\beta_-$  approaches zero.

Deriving general stability constraints is difficult since  $\mathcal{A}$  is a complicated function of  $d_+$ ,  $d_-$ , and  $\beta_+$  in (41) or a function of  $d_-$ ,  $d_+$ , and  $\beta_-$  in (42). Nevertheless, if we omit the feedback from the coupling domain, that is,  $\kappa_-$  in (41) or  $\kappa_+$  in (42), a nice closed-form expression for stability constraint can be found in this best case. Therefore, in the general case the coupling is not absolutely stable. Details are given in Section 4.

### 3.2 Partially implicit flux coupling with implicit time stepping

Like the explicit case, the partially implicit flux computation allows the two components to be handled simultaneously. But the equation corresponding to the interface node needs an implicit solve. The full algorithm is

$$q_{0_+}^{n+1} = b(T_{\frac{1}{2}}^{n+1} - T_{-\frac{1}{2}}^n) \quad (46a)$$

$$T_{j+\frac{1}{2}}^{n+1} - T_{j+\frac{1}{2}}^n = \frac{\Delta t}{\rho_+ c_+ \Delta z_+} (q_{j+1}^{n+1} - q_j^{n+1}), \quad j \geq 0 \quad (46b)$$

$$q_{0_-}^{n+1} = b(T_{\frac{1}{2}}^n - T_{-\frac{1}{2}}^{n+1}) \quad (46c)$$

$$T_{j+\frac{1}{2}}^{n+1} - T_{j+\frac{1}{2}}^n = \frac{\Delta t}{\rho_- c_- \Delta z_-} (q_{j+1}^{n+1} - q_j^{n+1}), \quad j < 0. \quad (46d)$$

Inserting the normal mode solution (37) into Equation (46), we have

$$\begin{aligned} 1 - \mathcal{A}^{-1} &= d_+ (\kappa_+ - 2 + \kappa_+^{-1}) \\ 1 - \mathcal{A}^{-1} &= d_+ (\kappa_+ - 1) - \beta_+ (1 - \mathcal{A}^{-1} \kappa_-^{-1} \kappa_+^{-1}) \\ 1 - \mathcal{A}^{-1} &= \beta_- (\mathcal{A}^{-1} \kappa_- \kappa_+ - 1) - d_- (1 - \kappa_-^{-1}) \\ 1 - \mathcal{A}^{-1} &= d_- (\kappa_- - 2 + \kappa_-^{-1}). \end{aligned} \quad (47)$$

The second and third equations give

$$\mathcal{A} = \frac{1 + \beta_+ \kappa_-^{-1} \kappa_+^{-1}}{\beta_+ + 1 - d_+ (\kappa_+ - 1)} \quad (48)$$

and

$$\mathcal{A} = \frac{1 + \beta_- \kappa_- \kappa_+}{\beta_- + 1 - d_- (\kappa_-^{-1} - 1)}, \quad (49)$$

respectively. We distinguish between two situations:  $|\kappa_-^{-1} \kappa_+^{-1}| \leq 1$  or  $|\kappa_- \kappa_+| \leq 1$ . For the former case, we can observe that

$$|1 + \beta_+ \kappa_-^{-1} \kappa_+^{-1}| \leq 1 + \beta_+$$

and

$$|\beta_+ + 1 - d_+ (\kappa_+ - 1)| > 1 + \beta_+.$$

Thus we have  $|\mathcal{A}| < 1$ . This is also true for the latter case. Therefore, the system is unconditionally stable.

#### 4 Analysis for one-way coupled model

In this section, we present a stability analysis of a one-way coupled diffusion model, which is forced by the other component in the coupled system but does not provide feedback to the forcing component [5]. In other words, one of the domains treats the variables from the other domain as a boundary condition. The advantage of using this simpler system is to enable explicit derivation of the stability criterion, and therefore give insight into the coupled stability. Again, we analyze the changes to stability induced by different treatments of the interfacial flux.

##### 4.1 Stability analysis for the diffusion equation

Let us consider the forced diffusion equation solely on the negative domain, as is expressed by

$$\frac{\partial}{\partial t} T_- = \frac{\partial}{\partial z} \left( K_- \frac{\partial}{\partial z} T_- \right), \quad z < 0 \quad (50a)$$

$$K_- \frac{\partial}{\partial z} T_- = b(T_+ - T_-), \quad z = 0. \quad (50b)$$

Explicit coupling boundary yields

$$T_{j+\frac{1}{2}}^{n+1} - T_{j+\frac{1}{2}}^n = \frac{\Delta t}{\rho_- c_- \Delta z_-} \left( q_{j+1}^{n+1} - q_j^{n+1} \right), \quad j < 0 \quad (51a)$$

$$q_j^{n+1} = \nu_- \frac{T_{j+\frac{1}{2}}^{n+1} - T_{j-\frac{1}{2}}^{n+1}}{\Delta z_-}, \quad q_0^{n+1} = b(T_{\frac{1}{2}}^n - T_{-\frac{1}{2}}^n). \quad (51b)$$

In the simplest case of ocean alone, for stability analysis, we can have a fixed boundary that is set to  $T_{\frac{1}{2}}^n = 0$  so that

$$q_0^{n+1} = -bT_{-\frac{1}{2}}^n. \quad (52)$$

Then the method for solving the diffusion equation can be written as

$$T_{j+\frac{1}{2}}^{n+1} - T_{j+\frac{1}{2}}^n = d_- \left( T_{j+\frac{3}{2}}^{n+1} - 2T_{j+\frac{1}{2}}^{n+1} + T_{j-\frac{1}{2}}^{n+1} \right), \quad j < -1 \quad (53a)$$

$$T_{-\frac{1}{2}}^{n+1} - T_{-\frac{1}{2}}^n = -\beta_- T_{-\frac{1}{2}}^n - d_- \left( T_{-\frac{1}{2}}^{n+1} - T_{j-\frac{3}{2}}^{n+1} \right), \quad j = -1. \quad (53b)$$

If there is no boundary, we can consider the solution

$$T_{j+\frac{1}{2}}^{n+1} = \mathcal{A}^{n+1} e^{i(jm\Delta z_-)}, \quad (54)$$

so that

$$\begin{aligned} \mathcal{A}^{n+1} e^{imj\Delta z_-} (1 - \mathcal{A}^{-1}) &= d_- \mathcal{A}^{n+1} e^{imj\Delta z_-} (e^{im\Delta z_-} - 2 + e^{-im\Delta z_-}), \quad j < -1 \\ \Rightarrow 1 - \mathcal{A}^{-1} &= d_- (e^{im\Delta z_-} - 2 + e^{-im\Delta z_-}) = 2d_- (\cos(m\Delta z_-) - 1) \\ \Rightarrow \mathcal{A}^{-1} &= 1 + 2d_- (1 - \cos(m\Delta z_-)) > 1, \end{aligned}$$

which results in an unconditionally stable scheme that is in agreement with the classical theory.

With the boundary condition, we establish the following theorem for the stability condition.

**Theorem 1** *Method (53) applied to the diffusion model (2b) yields a stable solution if and only if  $\beta_- \leq 1 + \sqrt{1 + 2d_-}$ .*

*Proof* We can no longer assume a solution of form (54). Instead, we assume the eigen-solution of the form

$$T_{j+\frac{1}{2}}^{n+1} = \mathcal{A}^{n+1} \kappa_-^j. \quad (55)$$

A stable solution that satisfies the far-field boundary condition (at  $j \rightarrow -\infty$ ,  $\kappa_-^j \rightarrow 0$ ) is  $|\kappa_-| > 1$  and  $|\mathcal{A}| \leq 1$ . From (53) we have

$$1 - \mathcal{A}^{-1} = d_- (\kappa_- - 2 + \kappa_-^{-1}) \quad (56a)$$

$$1 - \mathcal{A}^{-1} = -\beta_- \mathcal{A}^{-1} - d_- (1 - \kappa_-^{-1}), \quad (56b)$$

which gives

$$\kappa_-^{-1} = \frac{d_- + 1 + (\beta_- - 1)\mathcal{A}^{-1}}{d_-}. \quad (57)$$

Substituting into (56a), we have an equation for  $\mathcal{A}$ ,

$$d_- \mathcal{A}^2 - (\beta_- + d_-)\mathcal{A} - \beta_- (\beta_- - 1) = 0, \quad (58)$$

with roots

$$\mathcal{A} = \frac{(\beta_- + d_-) \pm \sqrt{(\beta_- + d_-)^2 + 4\beta_- (\beta_- - 1)d_-}}{2d_-}, \quad (59)$$

which are both real because under the radical is a positive real number.

Now we show that choosing the positive sign does not lead to a stable solution. First, we can observe from (57) that  $\kappa_-$  is also real. When choosing the positive sign, we have  $0 < \mathcal{A} \leq 1$ , and thus  $1 - \mathcal{A}^{-1} \leq 0$ . According to (57), the right-hand

side must be no larger than zero, which means  $k_- \leq 0$ . Equation (57) indicates that  $k_-$  can be negative or zero only when  $\beta_- \leq 1$ .

With  $\beta_- \leq 1$  and (59), we obtain

$$\begin{aligned} \mathcal{A} &= \frac{(\beta_- + d_-) + \sqrt{(\beta_- + d_-)^2 + 4\beta_-(\beta_- - 1)d_-}}{2d_-} \\ &\geq \frac{(\beta_- + d_-) + \sqrt{(\beta_- + d_-)^2}}{2d_-} > 1 + \frac{\beta_-}{d_-} > 1, \end{aligned}$$

which contradicts the assumption  $|\mathcal{A}| \leq 1$ .

Selecting the root with negative sign in (59), we consider the following two cases:

1. If  $\beta \geq 1$ , the condition  $|\mathcal{A}| \leq 1$  implies

$$\beta_-^2 - 2\beta_- - 2d_- \leq 0. \quad (60)$$

Solving the quadratic inequality gives

$$\beta_- \leq 1 + \sqrt{1 + 2d_-}. \quad (61)$$

2. If  $\beta < 1$ , we have a stable solution because

$$\begin{aligned} \mathcal{A} &= \frac{(\beta_- + d_-) - \sqrt{(\beta_- + d_-)^2 + 4\beta_-(\beta_- - 1)d_-}}{2d_-} \\ &< \frac{(\beta_- + d_-) - \sqrt{(\beta_- - d_-)^2}}{2d_-} \leq \frac{(\beta_- + d_-) - |\beta_- - d_-|}{2d_-} \\ &\leq \frac{(\beta_- + d_-) - \beta_- + d_-}{2d_-} = 1. \end{aligned}$$

Combining these two cases, we can see that  $\beta_- \leq 1 + \sqrt{1 + 2d_-}$  is the final condition for stability.

In Figure 3 we illustrate the stability regions resulting from our analysis. The norm of  $A$  and  $\kappa^{-1}$  are calculated for a range of values of  $\beta_-$  and  $d_-$  according to the expressions (59) and (57). The boundary of the stability regions agrees exactly with the relationship established by the analysis.

Based on the same model problem, Beljaars et al. derived an empirical stability boundary of  $\beta_- \leq 2 + \sqrt{d_-}^{-1.1}$  in [5], which is close to our analytical result. So, if there is no mixing, the explicit scheme is stable for weak coupling but unstable for strong coupling.

Even a decrease of stepsize  $\Delta t$  for the negative domain is not effective in suppressing coupling, because it reduces both  $d_-$  and  $\beta_-$ . Instead, the most effective way to suppress coupling instability is to reduce  $\Delta z_-$ , which increases  $d_-$  much more rapidly than  $\beta_-$ .

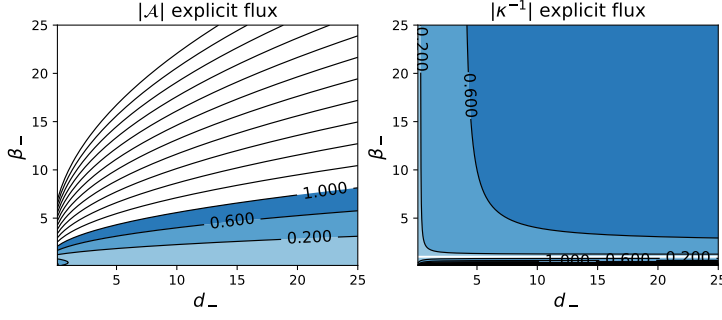


**Fig. 3** Stability regions for explicit flux coupling (based on analytical formula).

#### 4.2 Implicit interfacial flux

Next we consider the implicit treatment of the interfacial flux. The equation for the boundary node  $j = -1$  changes to

$$T_{-\frac{1}{2}}^{n+1} - T_{-\frac{1}{2}}^n = -\beta_- T_{-\frac{1}{2}}^{n+1} - d_- \left( T_{-\frac{1}{2}}^{n+1} - T_{j-\frac{3}{2}}^{n+1} \right), \quad j = -1. \quad (62)$$

Plugging (55) into (62), we have

$$1 - \mathcal{A}^{-1} = -\beta_- - d_- (1 - \kappa_-^{-1}). \quad (63)$$

Then we can solve (63) and (56a) for  $\kappa_-^{-1}$ .

After some manipulation, we obtain

$$\mathcal{A} = \frac{\beta_- - d_-}{\beta_- - d_- + \beta_-^2}, \quad \kappa_-^{-1} = \frac{d_-}{d_- - \beta_-}. \quad (64)$$

**Theorem 2** *The method (53) with the equation for the interface node replaced by (62) gives a stable solution of the one-way coupled diffusion model (2b).*

*Proof* 1. If  $\beta_- \geq d_-$ ,  $|\mathcal{A}| \leq 1$  always holds.

2. If  $\beta_- < d_-$ ,  $|\mathcal{A}| \leq 1$  leads to

$$\beta_-^2 + 2\beta_- - 2d_- \geq 0 \quad (65)$$

which reduces to

$$\beta_- \geq \sqrt{1 + 2d_-} - 1 \quad (66)$$

Combining these two cases, we have

$$\beta_- \geq \sqrt{1 + 2d_-} - 1 \quad (67)$$

For  $|\kappa_-^{-1}| \leq 1$ , we have

$$\beta_- \geq 2d_-. \quad (68)$$

Since  $2d_- > \sqrt{1 + 2d_-} - 1$ ,  $|\mathcal{A}| \leq 1$  always holds for all the eigen modes with  $|\kappa_-^{-1}| \leq 1$ , thus stability follows.

Figure 4 graphically depicts the stability conditions for the implicit case that are calculated directly using (64). It clearly shows that the region where  $|\kappa_-^{-1}| \leq 1$  is a subset of region where  $|\mathcal{A}| \leq 1$ .

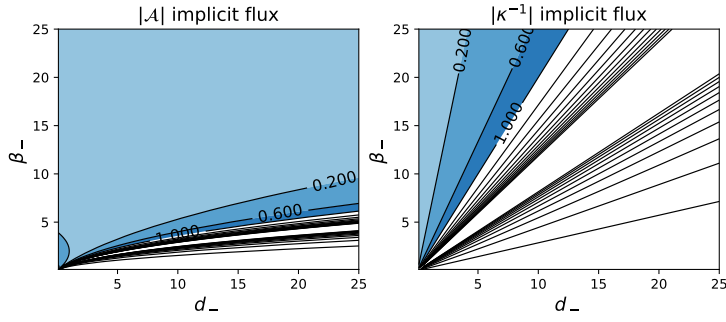


**Fig. 4** Stability regions for implicit flux coupling (based on analytical formula).

## 5 Numerical validation via matrix stability analysis

While the normal mode analysis provides insights into the stability of the coupled algorithms, we use a matrix stability analysis as a numerical tool to validate the results. To incorporate the influence of flux coupling in a simple way, we cast the partitioned algorithms in a monolithic framework that consists of each component and provides a unified view for different coupling approaches.

Depending on the flux coupling strategies, the interfacial fluxes  $q_{\frac{1}{2}}$  and  $q_{-\frac{1}{2}}$  can be computed in different ways. However, we can rewrite the fully discretized equation for (10) in a general matrix form

$$\mathbf{A}\mathbf{T}^{n+1} = \mathbf{B}\mathbf{T}^n. \quad (69)$$

Here  $\mathbf{T}$  is represented as

$$\mathbf{T} = [T_{N_-}, \dots, T_{-2}, T_{-1}, T_0, T_1, T_2, \dots, T_{N_+}]^T \quad (70)$$

for the Dirichlet-Neumann condition and

$$\mathbf{T} = [T_{N_-}, \dots, T_{-2}, T_{-1}, T_1, T_2, \dots, T_{N_+}]^T \quad (71)$$

for bulk condition due to the differences in the grid settings. In the following, we present the results for the bulk interface condition and then the Dirichlet-Neumann condition. Both the two-way coupled and the one-way coupled models are included



	Parameter	Description	Value	Unit
Atmosphere	$\rho_+$	density	1	$\text{kg m}^{-3}$
	$c_+$	heat capacity	1000	$\text{J kg}^{-1} \text{K}^{-1}$
	$\nu_+$	dynamic diffusivity	[300, ?]	$\text{J s}^{-1} \text{m}^{-1} \text{K}^{-1}$
	$K_+$	eddy diffusivity	[0.3, ?]	$\text{m}^2 \text{s}^{-1}$
	$n_+$	grid points	10	
	$d_+$	parabolic CFL	0.5	
Ocean	$\rho_-$	density	1000	$\text{kg m}^{-3}$
	$c_-$	heat capacity	4000	$\text{J kg}^{-1} \text{K}^{-1}$
	$\nu_-$	diffusion coefficient	$[4 \times 10^5, ?]$	$\text{m}^2 \text{s}^{-1}$
	$n_-$	grid points	20	
	$d_-$	parabolic CFL	100	
	$b$	bulk coefficient	[5, 100]	$\text{J s}^{-1} \text{m}^{-2} \text{K}^{-1}$

**Table 1** Typical parameters in practice. The smallest diffusivity coefficients are of particular interest. This is because instability is more likely to appear in these regime.

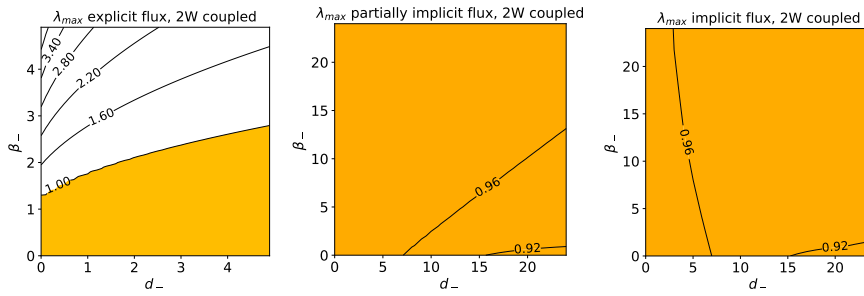


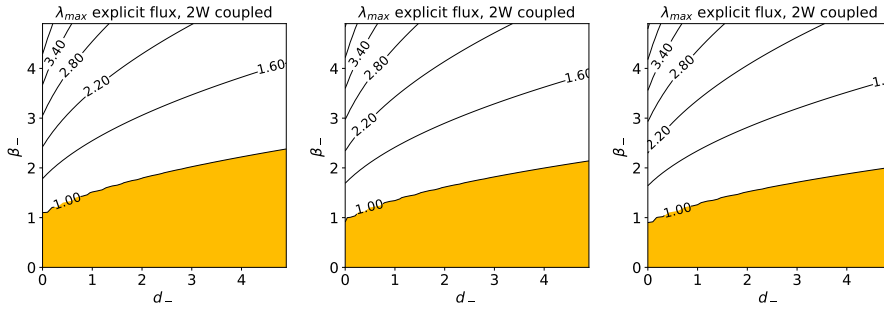
**Fig. 5** Stability regions for various flux coupling strategies with fixed parameters  $\beta_+ = 1.125$  and  $d_+ = 2.025$  for the coupling component.

$\lambda_{max} = \max(|\text{eig}(\mathbf{M})|)$  as a function over the Courant numbers  $\beta_-$  and  $d_-$  for the negative domain while fixing  $\beta_+$  and  $d_+$ . Figure 5 shows that using explicit flux coupling does not lead to absolute stability, a result that agrees with the finding in Section 3.1 for the coupled system. And as expected, both partially implicit flux coupling and implicit flux coupling can make the coupling unconditionally stable.

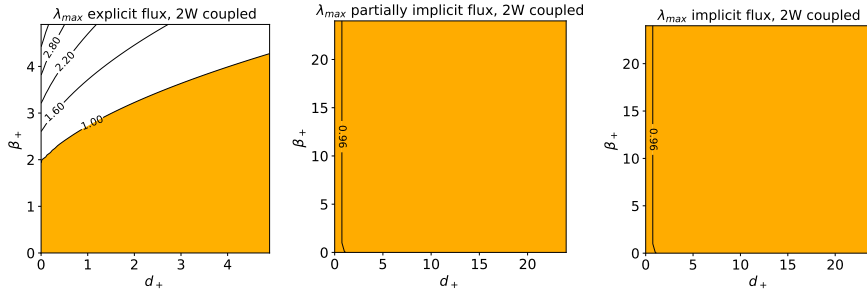
To investigate contributions of the positive domain to stability, we vary  $\beta_+$  and  $d_+$  by changing the grid size. As shown in Figure 6, the stability regions for the explicit flux coupling shrink as  $\beta_+$  and  $d_+$  increase.

Figure 7 shows the stability regions defined by  $\beta_+$  and  $d_+$  with fixed  $\beta_-$  and  $d_-$ . The stability region for the explicit flux coupling is larger than that obtained from the negative domain in Figure 5. For some other values of  $\beta_-$  and  $d_-$ , as shown in Figure 8, the stability region appears almost unchanged. The reason is that the negative domain is in a stable regime  $\beta_- \ll d_-$  and the effect of the upper right block of  $\mathbf{B}$  to the eigenvalues of  $\mathbf{M}$  is insignificant.

All the experiments for explicit flux coupling show that the classical absolute stability (independent of  $d_{\pm}$ ) can be recovered in the limiting case  $\beta_-$  or  $\beta_+$  approaches zero, as predicted by the analysis in Section 3.1.



**Fig. 6** Stability regions for explicit flux coupling with fixed parameters  $(\beta_+, d_+)$  set to  $(2.375, 9.025)$ ,  $(4.875, 38.025)$ ,  $(9.875, 156.025)$  from left to right for the coupling component.



**Fig. 7** Stability regions for various flux coupling strategies with fixed parameters  $\beta_- = 0.005938$  and  $d_- = 9.025$  for the coupling component.

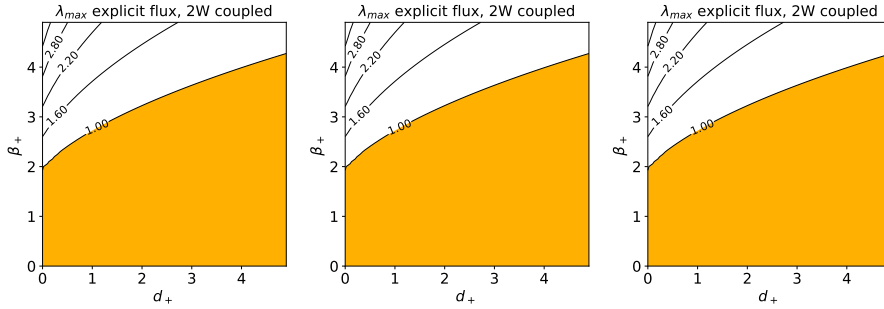


**Fig. 8** Stability regions for explicit flux coupling with fixed parameters  $(\beta_-, d_-)$  set to  $(0.012188, 38.025)$ ,  $(0.024688, 156.025)$ ,  $(0.049688, 632.025)$  from left to right for the coupling component.

### 5.1.2 One-way coupled model

Figure 9 plots the stability regions for the one-way coupled model according to the matrix stability analysis. It agrees with the theoretical prediction depicted in Figure 3. Interestingly, it also matches one of the two scenarios shown for the two-way coupled system (see Figure 8) but differs significantly from the other scenario (see Figure 6). These results indicate that the analysis for the one-way coupled

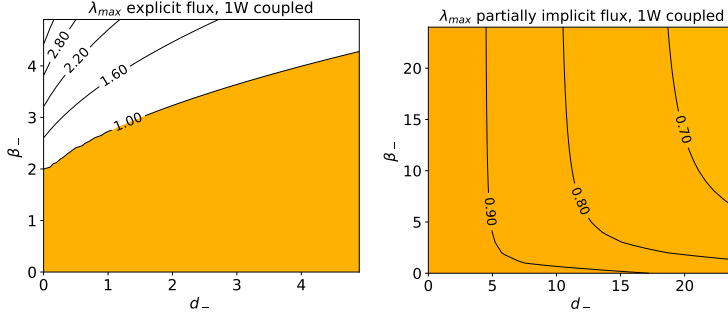


**Fig. 9** Stability regions for explicit flux coupling (left) and partially implicit flux coupling (right).

model with an assumption of fixed boundary  $T_{\frac{1}{2}}^n = 0$  gives a good approximation to the coupled scenario when the coupling component is in a stable regime where the bulk Courant number  $\beta$  is much less than the diffusion Courant number  $d$ .

Therefore, the analysis based on the one-way coupled model in Section 4 makes sense for atmosphere models forced by ocean models but may not be ideal for the ocean model because the heat capacity of atmosphere is much smaller and atmospheric dynamics evolves more rapidly, leading to a small bulk Courant number  $\beta$ .

This observation can also be explained from the matrix analysis perspective. In the case  $(\theta, \gamma) = (0, 0)$  and  $\beta_-$  negligible, the stability matrix can be denoted compactly as

$$\mathbf{M} = \begin{bmatrix} A_{11} & 0 \\ 0 & A_{22} \end{bmatrix}^{-1} \begin{bmatrix} B_{11} & 0 \\ B_{21} & B_{22} \end{bmatrix} = \begin{bmatrix} A_{11}^{-1}B_{11} & 0 \\ A_{22}^{-1}B_{21} & A_{22}^{-1}B_{22} \end{bmatrix}, \quad (73)$$

where  $\mathbf{M} \in \mathbb{R}^{n \times n}$ ,  $A_{11}, B_{11} \in \mathbb{R}^{k \times k}$ ,  $A_{22}, B_{22} \in \mathbb{R}^{(n-k) \times (n-k)}$ ,  $B_{21} \in \mathbb{R}^{(n-k) \times n}$ . Then the eigenvalues  $\lambda$  of  $\mathbf{M}$  must be roots of  $\det(\mathbf{M} - \lambda \mathbf{I}_n) = 0$ . We can see that  $\det(\mathbf{M} - \lambda \mathbf{I}_n) = \det(A_{11}^{-1}B_{11} - \lambda \mathbf{I}_k) \det(A_{22}^{-1}B_{22} - \lambda \mathbf{I}_{n-k})$ . Therefore, the spectrum of  $\mathbf{M}$  is the union of the spectrum of  $A_{11}^{-1}B_{11}$  and that of  $A_{22}^{-1}B_{22}$ . If the coupling domain (corresponding to  $A_{22}^{-1}B_{22}$ ) is in the stable regime, then the boundary of the stability region of the coupled system is determined by the spectrum of  $A_{11}^{-1}B_{11}$ .

For general cases where  $\beta_-$  is not negligible in the coupled system, one can use the Schur complement to obtain  $\det(\mathbf{M} - \lambda \mathbf{I}_n) = \det(A_{11}^{-1}B_{11} - \lambda \mathbf{I}_k) \det(A_{22}^{-1}B_{22} - \lambda \mathbf{I}_{n-k} - A_{22}^{-1}B_{21}(A_{11}^{-1}B_{11} - \lambda \mathbf{I}_k)^{-1}A_{11}^{-1}B_{12})$ , if  $B_{11}$  is invertible. Clearly, the spectral radius of  $\mathbf{M}$  depends on the spectral radii of  $A_{11}^{-1}B_{11}$  and its Schur complement matrix in  $\mathbf{M}$ . Further, given that  $A_{11}^{-1}B_{11}$  and  $A_{22}^{-1}B_{22}$  are stable,  $\mathbf{M}$  is not necessarily stable. This result implies that the stability region for the one-way coupled model is the best limiting case of stability regions for the two-way coupled model.

## 5.2 Dirichlet-Neumann condition

The matrix form of the CSS algorithm (10) with explicit coupling flux and the Dirichlet-Neumann condition exhibits a similar structure. For the purely explicit



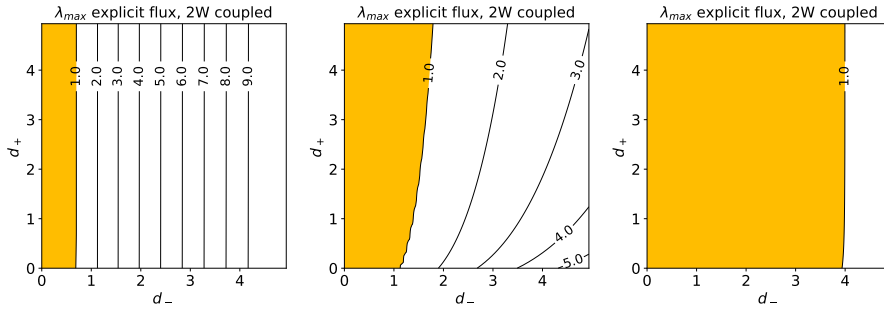


**Fig. 11** Stability regions for implicit integration methods with explicit flux coupling and Dirichlet-Neumann condition. From left to right,  $r = 2000, 1, 5e - 4$  respectively.

## 6 Conclusion

The stability characteristics of common partitioned coupling algorithms for ocean-atmosphere interactions have been studied with normal mode analysis and matrix eigenvalue analysis. Three different flux coupling schemes with both explicit and implicit time-stepping methods have been analyzed. Because of the special modeling strategy of the interfacial physics in climate models, the bulk interface condition is the focus of this work, although the classic Dirichlet-Neumann condition that is widely used for FSI problems is also included for completeness.

We show that the Dirichlet-Neumann condition imposed on the two coupled components does not affect stability for a purely explicit scheme but becomes a critical factor for an implicit method with explicit updating of the interfacial flux. The influence of the bulk interface condition is characterized with a variable that is formally similar to the Courant number. We show that the coupled system is unconditionally stable when partially implicit time-stepping methods are used for individual components and implicit flux coupling is used for interface nodes. In addition, we derive CFL-like stability conditions for the one-way coupled system and discuss the links between one-way and two-way coupled systems. The theory is supported by numerical experiments based on matrix eigenvalue analysis. Our results suggest that stability analysis of the one-way coupled model should be used with caution: it is most effective when used to reflect the stability behavior of the two-way coupled model when the bulk Courant number of the coupling component is small (e.g., atmospheric models forced by ocean models).

The results of the analysis performed for the 1D diffusion model is also applicable to real 3D models, because the heat and turbulence in the ocean-atmosphere circulation transfer mainly in the vertical direction. A general circulation model can be considered to be a collection of many single-column models, each of which may be associated with different bulk Courant numbers due to variability in surface dynamics. Therefore, numerical instability issues may arise in a subset of the models. Our analysis potentially provides a framework to identify where instability may occur, and the results can be used as guidelines for choosing proper flux coupling strategies and developing new time-stepping methods with better stability properties.

## References

1. Aggul, M., Connors, J.M., Erkmén, D., Labovsky, A.E.: A defect-deferred correction method for fluid-fluid interaction. *SIAM Journal on Numerical Analysis* **56**(4), 2484–2512 (2018). DOI 10.1137/17M1148219
2. Andreas, E.L., Horst, T.W., Grachev, A.A., Persson, P.O.G., Fairall, C.W., Guest, P.S., Jordan, R.E.: Parametrizing turbulent exchange over summer sea ice and the marginal ice zone. *Quarterly Journal of the Royal Meteorological Society* **136**(649), 927–943 (2010). DOI 10.1002/qj.618
3. Bao, J.W., Wilczak, J.M., Choi, J.K., Kantha, L.H.: Numerical simulations of air-sea interaction under high wind conditions using a coupled model: A study of Hurricane development. *Monthly Weather Review* **128**(7 I), 2190–2210 (2000). DOI 10.1175/1520-0493(2000)128<2190:NSOASI>2.0.CO;2
4. Bazilevs, Y., Calo, V.M., Hughes, T.J., Zhang, Y.: Isogeometric fluid-structure interaction: Theory, algorithms, and computations. *Computational Mechanics* **43**(1), 3–37 (2008). DOI 10.1007/s00466-008-0315-x
5. Beljaars, A., Dutra, E., Balsamo, G., Lemarié, F.: On the numerical stability of surface-atmosphere coupling in weather and climate models. *Geoscientific Model Development* **10**(2), 977–989 (2017). DOI 10.5194/gmd-10-977-2017
6. Bretherton, C.S., Battisti, D.S.: An interpretation of the results from atmospheric general circulation models forced by the time history of the observed sea surface temperature distribution. *Geophysical Research Letters* **27**(6), 767–770 (2000). DOI 10.1029/1999GL010910
7. Bryan, F.o., Kauffman, B.G., Large, W.G., Gent, P.R.: The NCAR CSM flux coupler. Technical Report NCAR/TN-424+STR, NCAR (1996)
8. Causin, P., Gerbeau, J.F., Nobile, F.: Added-mass effect in the design of partitioned algorithms for fluid-structure problems. *Computer Methods in Applied Mechanics and Engineering* **194**(42-44), 4506–4527 (2005). DOI 10.1016/j.cma.2004.12.005
9. Connors, J.M., Howell, J.S., Layton, W.J.: Partitioned time stepping for a parabolic two domain problem. *SIAM Journal on Numerical Analysis* **47**(5), 3526–3549 (2009). DOI 10.1137/080740891
10. Connors, J.M., Howell, J.S., Layton, W.J.: Decoupled time stepping methods for fluid-fluid interaction. *SIAM Journal on Numerical Analysis* **50**(3), 1297–1319 (2012). DOI 10.1137/090773362
11. Connors, J.M., Miloua, A.: Partitioned time discretization for parallel solution of coupled ODE systems. *BIT Numerical Mathematics* **51**(2), 253–273 (2011). DOI 10.1007/s10543-010-0295-z
12. Degroote, J., Bathe, K.J., Vierendeels, J.: Performance of a new partitioned procedure versus a monolithic procedure in fluid-structure interaction. *Computers and Structures* **87**(11-12), 793–801 (2009). DOI 10.1016/j.compstruc.2008.11.013
13. Edson, J.B., Jampana, V., Weller, R.A., Bigorre, S.P., Plueddemann, A.J., Fairall, C.W., Miller, S.D., Mahrt, L., Vickers, D., Hersbach, H.: On the exchange of momentum over the open ocean. *Journal of Physical Oceanography* **43**(8), 1589–1610 (2013). DOI 10.1175/JPO-D-12-0173.1
14. Fairall, C.W., Bradley, E.F., Rogers, D.P., Edson, J.B., Young, G.S.: Bulk parameterization of air-sea fluxes for tropical ocean/global atmosphere coupled-ocean atmosphere response experiment. *Journal of Geophysical Research C: Oceans* **101**(C2), 3747–3764 (1996). DOI 10.1029/95JC03205
15. Farhat, C., van der Zee, K.G., Geuzaine, P.: Provably second-order time-accurate loosely-coupled solution algorithms for transient nonlinear computational aeroelasticity. *Computer Methods in Applied Mechanics and Engineering* **195**(17-18), 1973–2001 (2006). DOI 10.1016/j.cma.2004.11.031
16. Giles, M.B.: Stability analysis of numerical interface conditions in fluid-structure thermal analysis. *International Journal for Numerical Methods in Fluids* **25**(4), 421–436 (1997). DOI 10.1002/(SICI)1097-0363(19970830)25:4<421::AID-FLD557>3.0.CO;2-J
17. Godunov, S.K., Ryaben'kii, V.S.: Spectral stability criteria of boundary value problems for non-self-adjoint difference equations. *Russian Mathematical Surveys* **18**(3), 1–12 (1963)
18. Golaz etc., J.: The DOE E3SM coupled model version 1: Overview and evaluation at standard resolution. *Journal of Advances in Modeling Earth Systems* (2019). DOI 10.1029/2018ms001603
19. Gustafsson, B., Kreiss, H.O., Sundström, A.: Stability theory of difference approximations for mixed initial boundary value problems. II. *Mathematics of Computation* **26**(119), 649–649 (1972). DOI 10.1090/S0025-5718-1972-0341888-3

20. Hallberg, R.: Numerical instabilities of the ice/ocean coupled system. *CLIVAR Exchanges* **19**(69), 38–42 (2014)
21. Hurrell, J.W., Holland, M.M., Gent, P.R., Ghan, S., Kay, J.E., Kushner, P.J., Lamarque, J.F., Large, W.G., Lawrence, D., Lindsay, K., Lipscomb, W.H., Long, M.C., Mahowald, N., Marsh, D.R., Neale, R.B., Rasch, P., Vavrus, S., Vertenstein, M., Bader, D., Collins, W.D., Hack, J.J., Kiehl, J., Marshall, S.: The community earth system model: A framework for collaborative research. *Bulletin of the American Meteorological Society* (2013). DOI 10.1175/BAMS-D-12-00121.1
22. Kreiss, H.O.: Stability theory for difference approximations of mixed initial boundary value problems, I. *Mathematics of Computation* **22**(104), 703–714 (1968)
23. Kudryavtsev, V., Chapron, B., Makin, V.: Impact of wind waves on the air-sea fluxes: A coupled model. *Journal of Geophysical Research: Oceans* (2014)
24. Kushnir, Y., Robinson, W., Blade, I., Hall, N., Peng, S., Sutton, R.: Atmospheric GCM response to extratropical SST anomalies: Synthesis and evaluation. *Journal of Climate* **15**(16), 2233–2256 (2002). DOI 10.1175/1520-0442(2002)015(2233:AGRTES)2.0.CO;2
25. Lemarie, F., Blayo, E., Debreu, L.: Analysis of ocean-atmosphere coupling algorithms: Consistency and stability. In: *Procedia Computer Science*, vol. 51, pp. 2066–2075. Elsevier (2015). DOI 10.1016/j.procs.2015.05.473
26. Liu, J., Zhang, Z., Horton, R.M., Wang, C., Ren, X.: Variability of North Pacific sea ice and East Asia-North Pacific winter climate. *Journal of Climate* **20**(10), 1991–2001 (2007). DOI 10.1175/JCLI4105.1
27. Liu, W.T., Katsaros, K.B., Businger, J.A., Liu, W.T., Katsaros, K.B., Businger, J.A.: Bulk parameterization of air-sea exchanges of heat and water vapor including the molecular constraints at the interface. *Journal of the Atmospheric Sciences* **36**(9), 1722–1735 (1979). DOI 10.1175/1520-0469(1979)036(1722:BPOASE)2.0.CO;2
28. Liu, Z., Zhang, Q., Wu, L.: Remote impact on tropical Atlantic climate variability: Statistical assessment and dynamic assessment. *Journal of Climate* **17**(7), 1529–1549 (2004). DOI 10.1175/1520-0442(2004)017(1529:RIOTAC)2.0.CO;2
29. Osher, S.: Stability of difference approximations of dissipative type for mixed initial-boundary value problems. *Mathematics of Computation* **23**, 335 (1969). DOI 10.1090/S0025-5718-1969-0246530-8
30. Perlin, N., Skillingstad, E.D., Samelson, R.M., Barbour, P.L.: Numerical simulation of air-sea coupling during coastal upwelling. *Journal of Physical Oceanography* **37**(8), 2081–2093 (2007). DOI 10.1175/JPO3104.1
31. Peterson, K., Bochev, P., Kuberry, P.: Explicit synchronous partitioned algorithms for interface problems based on lagrange multipliers. *Computers & Mathematics with Applications* **78**(2), 459 – 482 (2019). DOI <https://doi.org/10.1016/j.camwa.2018.09.045>. URL <http://www.sciencedirect.com/science/article/pii/S0898122118305637>
32. Roberts, A., Craig, A., Maslowski, W., Osinski, R., Duvivier, A., Hughes, M., Nijssen, B., Cassano, J., Brunke, M.: Simulating transient ice-ocean Ekman transport in the Regional Arctic System Model and Community Earth System Model. *Annals of Glaciology* **56**(69), 211—228 (2015). DOI 10.3189/2015AoS69A760
33. Roux, F.X., Garaud, J.D.: Domain decomposition methodology with Robin interface matching conditions for solving strongly coupled fluid-structure problems. *International Journal for Multiscale Computational Engineering* **7**(1), 29–38 (2009). DOI 10.1615/intjmultcompeng.v7.i1.50
34. Smith, S.D.: Coefficients for sea surface wind stress, heat flux, and wind profiles as a function of wind speed and temperature. *Journal of Geophysical Research: Oceans* **93**(C12), 15467–15472 (1988). DOI 10.1029/JC093iC12p15467
35. Yaglom, A.: Fluctuation spectra and variances in convective turbulent boundary layers: A reevaluation of old models. *Physics of Fluids* **6**(2), 962–972 (1994). DOI 10.1063/1.868328

The submitted manuscript has been created by UChicago Argonne, LLC, Operator of Argonne National Laboratory (“Argonne”). Argonne, a U.S. Department of Energy Office of Science laboratory, is operated under Contract No. DE-AC02-06CH11357. The U.S. Government retains for itself, and others acting on its behalf, a paid-up nonexclusive, irrevocable worldwide license in said article to reproduce, prepare derivative works, distribute copies to the public, and perform publicly and display publicly, by or on behalf of the Government. The Department of Energy will provide public access to these results of federally sponsored research in accordance with the DOE Public Access Plan. <http://energy.gov/downloads/doe-public-access-plan>.